Journal of
Materials Chemistry B

PAPER

View Article Online
View Journal

Cite this: DOI: 10.1039/c5tb02214b

A layered tungsten disulfide/acetylene black composite based DNA biosensing platform coupled with hybridization chain reaction for signal amplification

Hong-Lei Shuai, Ke-Jing Huang* and Ying-Xu Chen

Received 23rd October 2015,
Accepted 12th January 2016

DOI: 10.1039/c5tb02214b

www.rsc.org/MaterialsB

A 2-dimensional tungsten disulfide–acetylene black (WS_2–AB) composite is synthesized by a simple hydrothermal method to achieve excellent electrochemical properties for applications as a DNA biosensor. The biosensor is fabricated based on the Au nanoparticles (AuNPs) and WS_2–AB composite modified electrode, which subsequently is used to couple with a capture probe by an Au–S bond, then modified with target DNA, auxiliary DNA and bio-H1–bio-H2 (H1–H2) to perform hybridization chain reaction for signal amplification. Herein, two DNA hairpins H1 and H2 are opened by the recognition probe. The nicked double helices from hybridization chain reaction are used to immobilize horseradish peroxidase enzymes *via* biotin–avidin reaction, which produces signal-amplification detection of target DNA through the catalytic reaction of the hydrogenperoxide + hydroquinone system. Under optimum conditions, the as-prepared biosensor shows a good linear relationship between the current value and logarithm of the target DNA concentration ranging from 0.001 pM to 100 pM and a detection limit as low as 0.12 fM. Moreover, the fabricated biosensor exhibits good selectivity to differentiate the one-base mismatched DNA sequence. This work will open a pathway for ultrasensitive detection of other biorecognition events and gene-related diseases based on layered WS_2–AB and hybridization chain reaction.

1. Introduction

Ultrasensitive and highly selective detection of nucleic acids has attracted considerable interest and some assays have been developed for this purpose, such as fluorescence and electrochemical methods.[1,2] For example, Peng *et al.* have proposed a series of fluorescence methods for ultrasensitive detection of nucleic acids.[3–8] Electrochemical DNA sensors have gained particular attention due to their superior features of low cost, simplicity, portability and rapid response.[9] Since the DNA sequences of interest are present in very small amounts, it is essential to develop exponential amplification techniques that enable us to detect trace levels of a specific sequence.[10] Therefore, the development of signal amplification strategies to fabricate ultrasensitive DNA biosensors has recently received particular interest.[11,12] One of the signal amplification strategies is the post amplification strategy toward the signal produced by the hybridization event,[13] and it can improve on the sensitivity in the electrochemical detection of DNA by metal nanoparticles,[14] enzyme-aided reactions,[15] DNA biobarcodes[16] and redox indicators[17] as signal amplifying labels. As an advanced DNA assembly technology, hybridization chain reaction (HCR) has recently developed as an attractive tool for signal amplification toward DNA detection due to its significant advantages such as simple, cost-effective, sensitive and selective.[18] The target acts as an initiator to trigger the hybridization reaction during the course of HCR, which leads to the formation of a long-range of DNA sequence in a long nicked duplex DNA. The initiator triggered reaction generates a low pseudo-positive result, leading to a high signal to noise ratio. Furthermore, every target can trigger a HCR event to form a long-range DNA sequence, which shows great potential in the sensitive detection of DNA. It is worth mentioning that the products of HCR are highly ordered DNA double helices, which can precisely control density to combine signaling molecules. Until now, HCR has extensively been applied for signal-amplification detection of various analytes.[18,19]

Acetylene black (AB), a special kind of carbon black with a porous structure, has attracted a great amount of attention because of its extraordinary properties, such as high accumulation efficiency, excellent electric conductivity, large surface area, high catalytic activity and strong adsorptive ability.[20,21] It has been used for the fabrication of electrochemical sensors to improve the detection sensitivity and the response signal.[22,23]

Two-dimensional (2D) layered compounds have attracted immense interest in the field of electrochemistry in the past decade, such as WS_2, MoS_2, SnS_2, CoS_2 and VS_2. They have been

College of Chemistry and Chemical Engineering, Xinyang Normal University, Xinyang 464000, China. E-mail: kejinghuang11@163.com; Tel: +86-376-6390611

successfully established as a new paradigm in chemistry and biosensing due to their large surface area and fast heterogeneous electron transfer.[24–26] From the structural point of view, WS_2 is a typical member of 2D layered compounds. It is composed of a metal W layer sandwiched between two sulfur layers and stacked together by weak van der Waals interactions.[27] The layered structure of WS_2 is expected to act as an excellent functional material due to the fact that 2D electron correlations among W atoms would aid in enhancing planar electric transportation properties. In fact, WS_2 has attracted considerable attention due to its extensive applications as electrocatalysts, lubricants, lithium batteries, supercapacitors, and so on.[28–30] Nevertheless, less attention has been paid to its application as an electrode material for electrochemical sensing because the electronic conductivity of WS_2 is still relatively low, similar to the most transition metal oxides. To overcome this problem, hybrid materials that are used for the incorporation of WS_2 with good electronic conductive materials seem to be imperative.

In this work, a layered 2D tungsten disulfide/acetylene black (WS_2–AB) composite was synthesized by a simple hydrothermal method. An ultrasensitive electrochemical DNA biosensor was fabricated based on the Au nanoparticles (AuNPs) and a WS_2–AB composite modified glassy carbon electrode (GCE), which possessed low background current, good conductivity and large electroactive surface area. The probe ssDNA was linked to the modified electrode *via* an Au–S bond. Afterward, auxiliary DNA was immobilized on the modified electrode. The auxiliary DNA had sequence complementarity to target DNA and it may expedite target DNA to HCR with H1–H2 on the electrode surface and enhanced the selectivity of the sensor. The two DNA hairpins H1–H2 were opened by the recognition probe. The nicked double helices from hybridization chain reaction were used to immobilize horseradish peroxidase enzymes *via* biotin–avidin, which produced signal-amplification detection of target DNA through the catalytic reaction of the hydrogenperoxide + hydroquinone system. As a 2D layered nanostructure, the as-prepared WS_2–AB displayed a large effective surface area. This allowed more biomolecules (capture DNA) to be immobilized at the electrode surface, which reduced the distance for electron transfer and ion diffusion paths between the capture DNA and nanomaterials. As a result, the charge transfer to the electrodes became easier. In addition, the strong interactions between the capture DNA and the electrode surface enhanced the surface density of the immobilized analytes, which therefore led to a low detection limit. Under optimal experimental conditions, the proposed DNA biosensor showed a sub-femtomolar detection limit for the target DNA with a wide linear range and good selectivity.

2. Experimental

2.1. Reagents and apparatus

$K_3Fe(CN)_6$, $K_4Fe(CN)_6$ and chloroauric acid ($HAuCl_4 \cdot 4H_2O$) were purchased from Sigma-Aldrich (St. Louis, MO). The other chemicals were of analytical grade and used without further purification. All aqueous solutions were prepared using ultrapure water ($\geq$18.2 MΩ, Milli-Q, Millipore). All DNA sequences were synthesized by Shanghai Sangon Biological Engineering Technological Co. Ltd (China). The sequences of synthesized DNA are shown in Table 1 and the buffers used in this work are shown in Table 2.

All electrochemical measurements were performed on an EC550 electrochemical workstation (Wuhan, Gaoss Union, China) except that electrochemical impedance spectroscopy (EIS) measurements were carried out on an RST5200F electrochemical workstation (Zhengzhou Shi Rui Si Instrument China) with a conventional three-electrode system composed of a platinum wire as an auxiliary electrode, a saturated calomel electrode (SCE) as a reference electrode and a 3 mm diameter GCE as a working electrode. Nanostructures were characterized using a JEM 2100 transmission electron microscope (TEM, JEOL, Tokyo, Japan) and a Hitachi S-4800 scanning electron microscope (SEM, Tokyo, Japan). The X-ray diffraction (XRD) pattern was obtained on a model D/max-rA diffractometer (Rigaku, Japan). Raman spectra were recorded at ambient temperature on a Renishaw Raman system model 1000 spectrometer (Gloucestershire, UK). Fourier transform infrared

Table 1 DNA sequences employed in this work

Oligonucleotides	Sequences (5′–3′)
Capture probe	5′-TGCAGTTTCCGTCCGTAGTTTTT-SH-3′
Target DNA	5′-CTACGGACGGAAACTGCACCTGTATTCCCATACCCATCAT-3′
One-based mismatch DNA	5′-CTACGGACGGAAACTGCAACTGTATTCCCATACCCATCAT-3′
Three-based mismatch DNA	5′-CTACGGACGCAAACTGCAACTGTATTCTCATACCCATCAT-3′
Noncomplementary	5′-CTGCTTCCAAACCTTTAACATAGCCGCAAGCGTTAGCTGC-3
Auxiliary DNA	5′-AGTCTAGGATTCGGCGTGGGTTAAATGATGGGTATGGGAATACAGG-3′
Bio-H1	5′-biotin-TTAACCCACGCCGAATCCTAGACTCAAAGTAGTCTAGGATTCGGCGTG-3′
Bio-H2	5′-biotin-AGTCTAGGATTCGGCGTGGGTTAACACGCCGAATCCTAGACTACTTTG-3′

Table 2 Buffers used in this work

Buffer	Solute and pH	Application
1	PBS1 (10 mM PBS, 3 M NaCl and 2.7 mM KCl, pH 7.4)	Capture DNA
2	PBS2 (10 mM PBS, 150 mM NaCl, 2.7 mM KCl and 10 mM $MgCl_2$, pH 7.4)	Target DNA, Auxiliary DNA, Mismatch DNA
3	PBS3 (50 mM PBS and 1 M NaCl, pH 7.4)	Bio-H1, Bio-H2

(FT-IR) spectra were recorded on a Bruker-Tensor 27 IR spectrophotometer (Ettlingen, Germany).

2.2. Synthesis of WS_2, AB and WS_2–AB nanocomposites

WS_2 nanosheets were prepared according to a previous protocol.[31] Commercial WS_2 powder was first ground by ball grinding mill for 3 h. Subsequently, the WS_2 powder (40 mg) was added in 40 mL of sulfuric acid and refluxed for 24 h at 90 °C. The as-prepared products were collected by centrifugation and washed with water several times to remove the residual H_2SO_4. Finally, the WS_2 nanosheets were dried in a vacuum oven at 70 °C for 24 h.

AB was firstly treated with concentrated nitric acid. In short, 1.0 g AB was added in 200 mL of concentrated nitric acid and then refluxed at 140 °C for 2.0 h. After cooling, the black product was washed thoroughly with water until the pH was close to 7, and then dried at 80 °C for 24 h. WS_2–AB composites were synthesized by a simple hydrothermal method. Five WS_2–AB composites with mass ratios of WS_2 to AB of 0.5 : 1, 1 : 1, 1.5 : 1, 2 : 1 and 3 : 1 were synthesized as follows: firstly, 1 mg of WS_2 was ultrasonically dispersed in 40 mL of deionized water, and AB with different mass (0.5, 1.0, 1.5, 2.0 and 3.0 mg) was then added and ultrasonically dispersed for 30 min. After that, the mixture was diluted with water to 80 mL and transferred to a 100 mL Teflon-lined stainless steel autoclave and heated at 180 °C for 48 h. After cooling to room temperature naturally, the WS_2–AB nanocomposites were collected by centrifugation, washed with water several times, and finally dried in a vacuum oven at 80 °C for 24 h.

2.3. Preparation of a DNA biosensor and its electrochemical measurements

For electrode preparation, 1.0 mg of WS_2–AB nanocomposites were dispersed in 1 mL of water with ultrasonication for 20 min to get homogenous suspension (1 mg mL^{-1}). The bare GCE was polished sequentially with 0.3 and 0.05 μm alumina slurries, washed ultrasonically with water and ethanol and then dried with nitrogen gas. The WS_2–AB composite modified electrode was prepared by applying 6 μL of suspension onto the cleaned GCE and dried in air. For assembling the probe DNA, the AuNPs were electrodeposited on a WS_2–AB/GCE from a PBS (pH 7.0) solution containing 0.1% $HAuCl_4$ at a constant potential of −0.2 V for 60 s. After that, 8 μL of 0.5 μM probe DNA solution was dropped onto the AuNPs/WS_2–AB/GCE and allowed to react overnight. After being thoroughly washed with PBS to remove the unbound probe DNA, 8 μL of 1% BSA was dropped on the probe DNA/AuNPs/WS_2–AB/GCE surface for 30 min to eliminate nonspecific adsorption. After the electrode was rinsed with buffer solution, 8 μL of target DNA was applied on the BSA/capture probe/AuNPs/WS_2–AB/GCE and incubated for 90 min at 37 °C. Afterward, the auxiliary DNA was added on the electrode and incubated at 37 °C for 40 min. H1 and H2 samples were heated to 95 °C for 5 min and then allowed to cool to room temperature for 2 h. After that, the sample was diluted with PBS3 to the final concentration of 0.5 μM, and then 8 μL of the mixture was coated on the electrode and incubated at room temperature for 50 min for the HCR. 6 μL of avidin–HRP (0.5 μM mL^{-1}) was then dropped on the modified electrode and incubated for 35 min. Finally, the resulting avidin–HRP/auxiliary DNA/target DNA/BSA/capture probe/AuNPs/WS_2–AB/GCE was rinsed with distilled water and used for electrochemical measurements.

For DNA sensing, cyclic voltammetry (CV) was carried out in 0.1 M PBS (pH 7.0) containing 1.0 mmol L^{-1} $[Fe(CN)_6]^{3-/4-}$ and 0.1 mol L^{-1} KCl solution between a potential window of −0.2 V and 0.6 V with a scan rate of 100 mV s^{-1}. EIS measurements were performed in 0.1 M PBS (pH 7.0) containing 5.0 mmol L^{-1} $[Fe(CN)_6]^{3-/4-}$ and 0.1 mol L^{-1} KCl solution, with the AC voltage amplitude of 5 mV, the voltage frequencies from 100 KHz to 0.1 Hz and the applied potential of 0.2 V. The DPV measurements were conducted in the potential region from −0.4 V to 0.2 V (*vs.* SCE) in 0.1 M PBS (pH 7.0) containing 2 mM HQ and 1.8 mM H_2O using a pulse amplitude of 50 mV, pulse width of 50 ms and pulse period of 0.2 s.

3. Results and discussion

3.1. Design principle of the DNA biosensor

The principle of DNA biosensor fabrication is illustrated in Scheme 1. First, the 2D WS_2–AB composites are prepared and used as supporting substrates of the biosensor due to their large specific surface area and good electro-conductivity. After AuNPs are deposited on the WS_2–AB modified GCE, the designed thiolated probe DNA sequence which is complementary to target DNA is immobilized on the AuNPs/WS_2–AB/GCE to form an upright probe through the Au–S bond. In the presence of target DNA, the probe DNA can hybridize with target DNA on the electrode. After that, auxiliary DNA hybridizes with target DNA and the two species of DNA hairpins bio-H1 and bio-H2 are opened by the recognition probe, and hybridized one by one. In the present design, two complementary hairpins Bio-H1 and Bio-H2 are stable and would not open or hybridize each other at room temperature. Since the two hairpins are modified with biotin, lots of biotin can be introduced onto the electrode by the hybridization between auxiliary DNA and H1–H2. When the avidin–HRP is added, it can result in a strongly current response

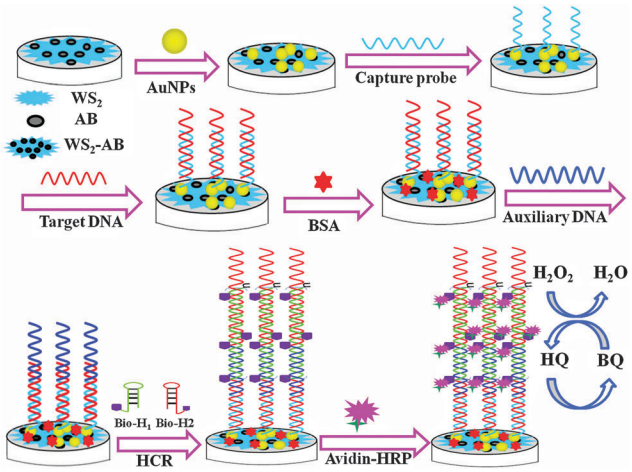

Scheme 1 Schematic illustration of the working principle of DNA detection based on the hybridization chain reaction.

by the catalysis of HRP to the mixture of H_2O_2 and HQ, and thus leads to the signal amplification.

3.2. Characterization

The morphologies of the as-prepared samples were characterized by SEM and TEM. Fig. 1A–C displays the SEM images of different samples. The SEM image in Fig. 1A reveals the layered WS_2 sheets, illustrating the flake-like shape of WS_2. The SEM image of AB is shown in Fig. 1B. Many nanocarbon oblate spheroids with diameters ranging from 20 to 50 nm are observed. The SEM image of WS_2–AB composites is shown in Fig. 1C. It shows that AB cumulates and distributes well on the 2D WS_2 skeleton, evidencing the well-behaved assembly process. This layered architecture is helpful to increase the specific surface area of the WS_2–AB composite, which is of benefit to load more cDNA and therefore leads to a low detection limit of analytes.

In order to reveal the fine microstructure, the synthesized WS_2, AB and WS_2–AB composites were characterized by TEM and HRTEM. Fig. 1D shows the flake-like shape of WS_2. As shown in Fig. 1E, the AB exhibits the typical oblate spheroid structure. From Fig. 1F, it can be clearly seen that AB is cumulated and distributed on the layered WS_2. In the illustrations, the HRTEM image of WS_2–AB clearly shows that WS_2 has a linear lattice fringe and AB shows the typical lattice fringe of carbon material which is similar to fingerprints, indicating that AB distributed well on the WS_2 surface. The HRTEM images of WS_2–AB in Fig. 1G and H show that layered WS_2 has defects or disorder structures.

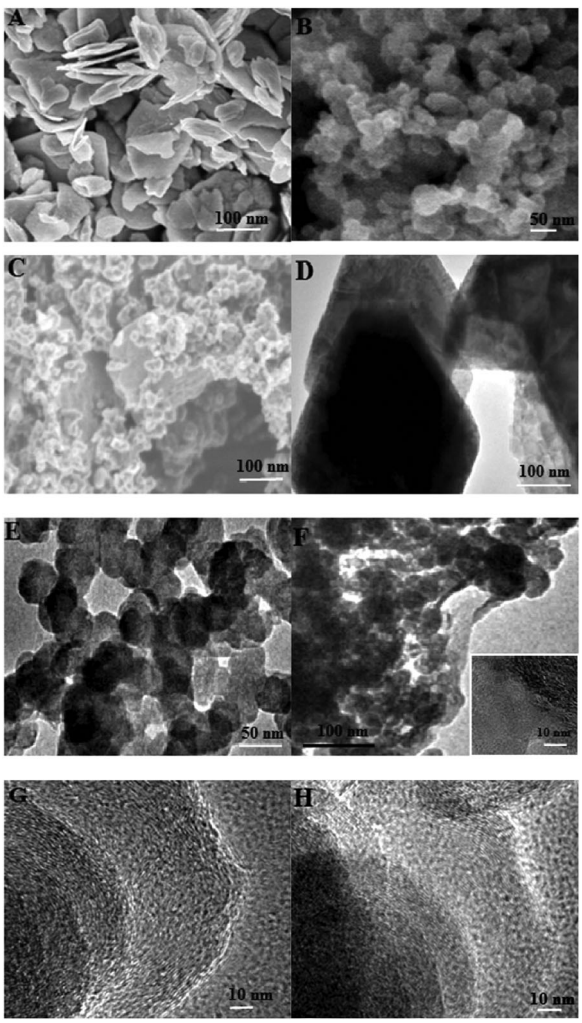

Fig. 1 SEM images of WS_2 (A), AB (B) and WS_2–AB composites (C); TEM images of WS_2 (D), AB (E) and WS_2–AB composites (F); HRTEM images of WS_2–AB composites (G and H).

The good dispersibility of the composites plays an important role in the construction of stable electrochemical sensors. Herein, WS_2, AB and WS_2–AB composites are dispersed in water by vigorous shaking. Fig. 2A shows that AB and WS_2–AB composites display the homogenous black solution and WS_2 nanosheets produce silvery grey solution. WS_2 and AB subside to the bottom after being allowed to stand for three days while the WS_2–AB composites still disperse well in water (Fig. 2B), indicating good dispersibility of the WS_2–AB composite.

Fig. 2C records the XRD patterns of WS_2, AB and WS_2–AB composites. It can be seen that diffraction of WS_2 alone shows the typical peaks at 14.3°, 28.9°, 32.7°, 33.5°, 39.8°, 43.9° and 49.6°, which correspond to (002), (004), (100), (101), (103), (006) and (105) planes of WS_2 (JCPDS No. 37-1492), respectively. Two broad diffraction peaks centered at about 25.7° and 42.5° corresponding to AB are observed. The main diffraction peaks of WS_2 are very weak, indicating that AB densely covered on the surface of WS_2 nanosheets. For WS_2–AB composites, the presence of diffraction peaks centered at 14.3°, 25.7°, 28.9°, 32.7°, 33.5°, 39.8°, 43.6° and 49.6° suggests a few-layered structure for WS_2 and AB.

Further insights into the structural and electronic properties of products were obtained from the Raman spectrum (Fig. 2D). The Raman spectrum of AB exhibits the *D* band at 1350 cm^{-1} that arises from sp^3-hybridized carbon and the *G* bands at 1590 cm^{-1} which represents the E_{2g} zone center mode of crystalline graphite. The characteristic bands of WS_2 observed at 709 cm^{-1} and 800 cm^{-1} correspond to the E_{2g} and A_{1g} modes, respectively. The WS_2–AB composites show the peaks at 1348 cm^{-1} and 1589 cm^{-1}, which are assigned to the *D* and *G* peaks of the AB and 709 cm^{-1} and 800 cm^{-1} correspond to the WoS_2, respectively, thus confirming the presence of AB and WS_2 in the composite and complete correspondence with the findings from the XRD diffraction studies.

FT-IR spectra of different samples were compared between 4000 and 500 cm^{-1}. As shown in Fig. 2E, no significant difference is observed between the spectra with respect to the wave number of major bands for the AB and WS_2–AB composites. The bond at 3425 cm^{-1} is mainly assigned to the stretching vibrations of the O–H bonds. The difference in the intensity of the OH vibration indicates that the free hydroxy groups increase after WS_2 combined with AB. This is helpful to increase the dispersibility of the WS_2–AB composite in water, and this characteristic helps us to develop stable electrochemical sensors. The weak peak at about 700 cm^{-1} at WS_2–AB and WS_2 spectra is assigned to W–S vibration.

3.3. Electrochemical characterization

As shown in Fig. 3A, the CV at the bare GCE shows the lowest reduction peak current of 12 μA (curve a). Five WS_2–AB

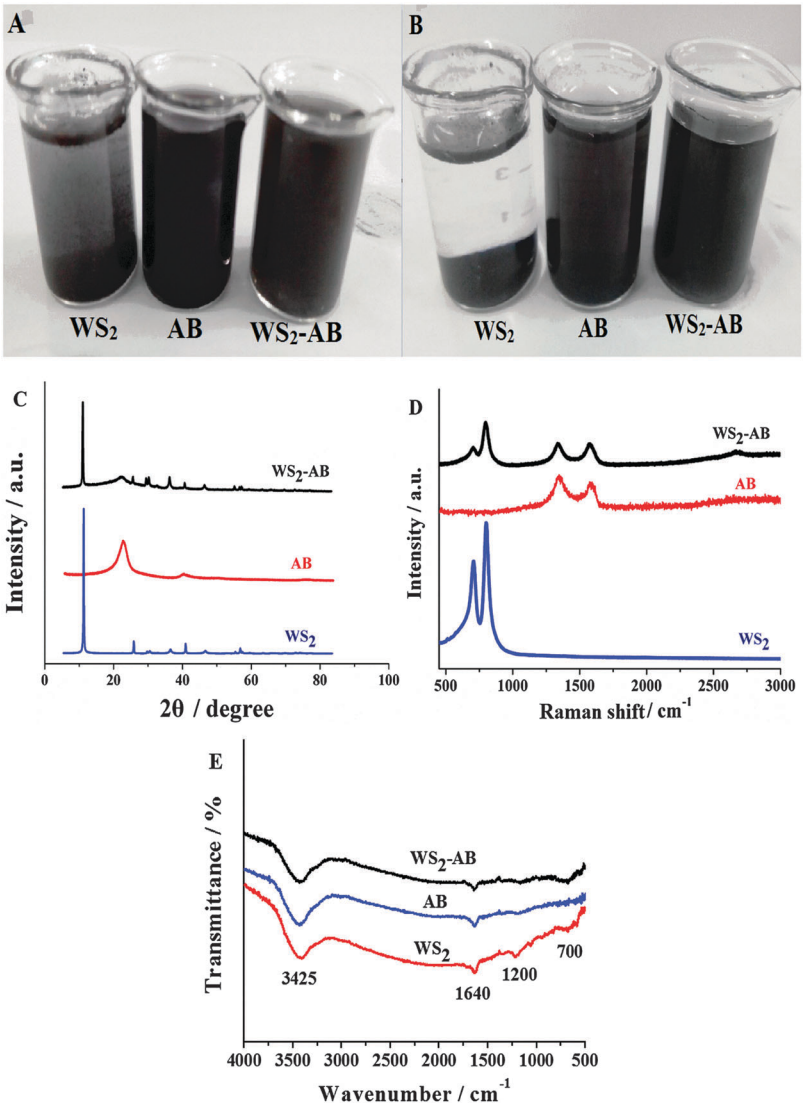

Fig. 2 (A and B) The photograph of WS_2, AB and WS_2–AB composite dispersed solution: (A) vigorous shaking for 30 min; (B) allowed to stand for three days; (C) XRD patterns of WS_2, AB and WS_2–AB composites; (D) Raman spectra of WS_2, AB and WS_2–AB composites; (E) FT-IR spectra of WS_2, AB and WS_2–AB composites.

composites with mass ratios of WS_2 to AB (0.5 : 1, 1 : 1, 1.5 : 1, 2 : 1 and 3 : 1) are applied on the GCE and five reduction peak currents of 28.1 μA (curve e), 31.3 μA (curve f), 23.5 μA (curve d), 18.7 μA (curve c) and 15.3 μA (curve b) are obtained, respectively. The electrode modified WS_2–AB composites with mass ratios of WS_2 to AB of 1 : 1 show the highest peak current. So they were used in the further experiments.

Fig. 3B shows the lowest reduction peak current of 12 μA at the bare GCE (curve a). The presence of AB on the GCE yields a reduction peak current of 19.4 μA (curve b) due to the reduced electron transfer resistance. When WS_2–AB composites are immobilized on the electrode, a corresponding peak current of 31.6 μA (curve c) is observed due to the large specific surface area and the good conductor of the composites. The highest reduction peak current (33.4 μA) obtained at the AuNPs/WS_2–AB/GCE (curve d) indicates that the synchronous introduction of WS_2–AB and AuNPs on the electrode effectively enhances the peak currents, which is due to the effective integration of individual advantages of WS_2–AB and AuNPs (such as large surface area and excellent electronic conductivity). In addition, the reduction peak current of the capture probe/WS_2–AB/GCE (curve e) obviously decreases due to the electrostatic repellence between negatively charged phosphate of DNA and negative charged $[Fe(CN)_6]^{3-/4-}$. The peak current of the BSA/capture probe/AuNPs/WS_2–AB/GCE (curve e) further decreases because BSA is a biological macromolecule, which hinders the electron exchange on the surface of the electrode. The peak current of the target DNA/BSA/capture probe/AuNPs/WS_2–AB/GCE (curve f), auxiliary DNA/target DNA/BSA/capture probe/AuNPs/WS_2–AB/GCE (curve h) and HCR/auxiliary DNA/target DNA/BSA/capture probe/AuNPs/WS_2–AB/GCE (curve i) gradually decreases due to specific binding among DNA. More and more DNA sequences are fixed on the electrode surface causing the DNA chain to extend and the electron transfer becomes more difficult.

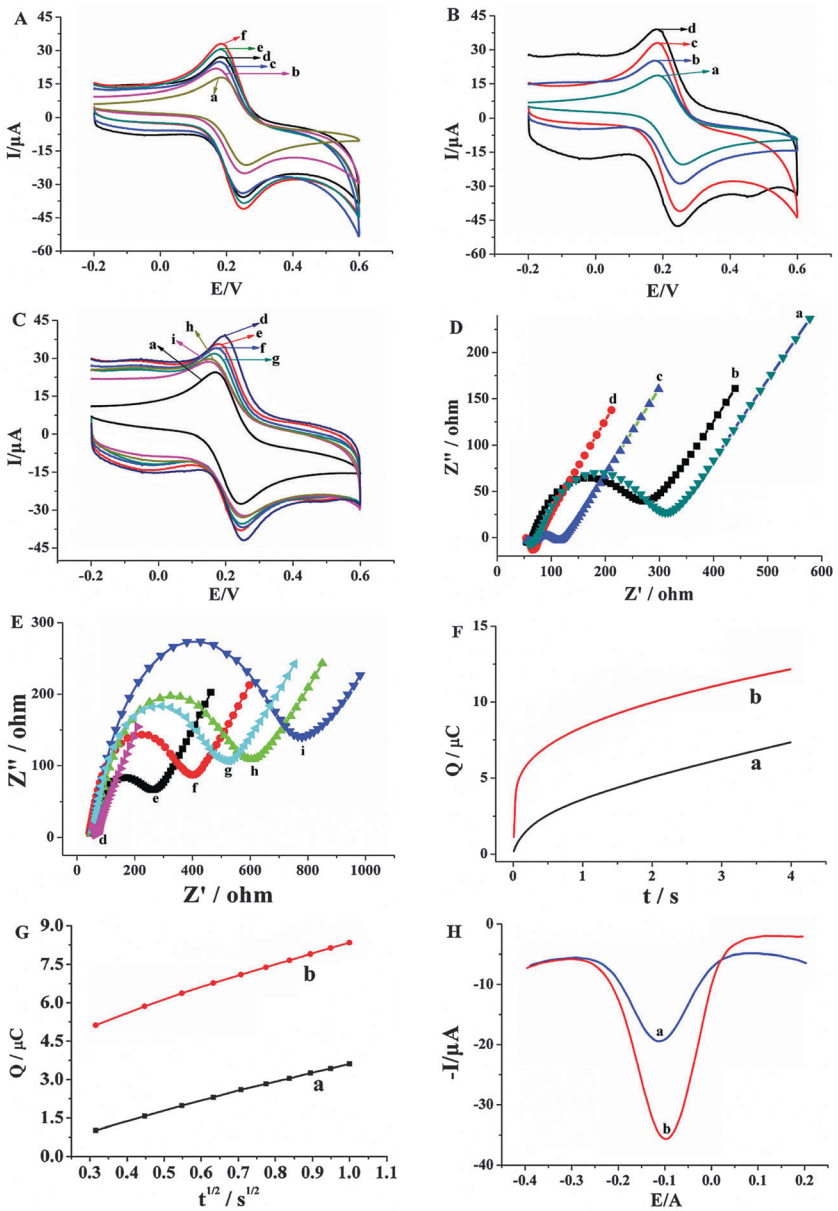

Fig. 3 (A) CVs of the GCE (a) and different mass ratios of WS_2 and AB in composites: 3 : 1 (b), 2 : 1 (c), 1.5 : 1 (d), 0.5 : 1 (e), 1 : 1 (f); CVs (B and C) and EIS (D and E) of the bare GCE (a), AB/GCE (b), WS_2–AB/GCE (c), AuNPs/WS_2–AB/GCE (d), capture probe/AuNPs/WS_2–AB/GCE (e), BSA/capture probe/AuNPs/WS_2–AB/GCE (f), target/capture probe/BSA/AuNPs/WS_2–AB/GCE (g), auxiliary/target/capture probe/BSA/AuNPs/WS_2–AB/GCE (h), HCR/auxiliary/target/capture probe/AuNPs/WS_2–MWCNTs/GCE (i). (F) Plot of Q–t curves of the bare GCE (a) and AuNPs/WS_2–AB/GCE (b) in 0.1 mM $K_3[Fe(CN)_6]$ containing 1.0 M KCl; (G) plot of Q–$t^{1/2}$ curves on GCE (a) and AuNPs/WS_2–MWCNTs/GCE (b); (H) DPVs of HRP/HCR/auxiliary/target/probe/BSA/AuNPs/GCE (a) and HRP/HCR/auxiliary/target/probe/BSA/AuNPs/WS_2–AB/GCE (b) in 0.1 M PBS (7.0) containing 1.8 mM H_2O_2 and 2 mM HQ.

EIS is one important tool for probing the features of surface-modified electrodes. In the impedance spectra, the increase in the diameter of the semicircle indicates the enhancement in the interfacial electron transfer resistance (R_{et}). When AB (curve b) or WS_2–AB composites (curve c) are applied on the GCE, R_{et} displays a smaller value than the bare GCE (curve a) due to their good conductivity (Fig. 3D). However, the R_{et} of WS_2–AB composites show the lowest value, indicating the good conductivity of WS_2–AB. When AuNPs are further electrodeposited on the WS_2–AB/GCE, the R_{et} decreases obviously with an almost straight line (curve d), which is ascribed to the excellent conductive ability of the AuNPs/WS_2–AB film. When the capture probe is further immobilized on the electrode (curve e), the R_{et} value increases greatly because of the electrostatic repulsion between anionic $[Fe(CN)6]^{3-/4-}$ and the negatively charged phosphate backbone (Fig. 3E). After being treated with BSA, the R_{et} value further decreases (curve f). Following the addition of target DNA results in the R_{et} increasing dramatically (curve g) due to the hybridization between target DNA and capture probes. Similarly, the R_{et} increases when auxiliary DNA is applied on the electrode surface (curve h). After HCR being triggered by the recognition probe with bio-H1 and bio-H2, R_{et} increases significantly (curve i) due to more DNAs being

immobilized on the electrode surface, which make the electron transfer become more difficult. These results indicated that the biosensor is effectively constructed.

The effective surface areas of the GCE and the AuNPs/WS_2–AB/GCE were compared by chronocoulometry in 0.1 mM $K_3[Fe(CN)_6]$ solution containing 1.0 M KCl, where the standard diffusion coefficient (D_0) of $K_3[Fe(CN)_6]$ at 25 °C is 7.6×10^{-6} cm^2 s^{-1}. The effective surface area (A) of electrodes is calculated according to the following equation:

$$Q = 2nFAcD^{1/2}t^{1/2}/\pi^{1/2} + Q_{dl} + Q_{ads} \quad (1)$$

where n is the number of electrons transferred, F (C mol^{-1}) is the Faraday constant, A (cm^2) is the area of the electrode, c (mol cm^{-3}) is the concentration of the substrate, D (cm^2 s^{-1}) is the diffusion coefficient, Q_{dl} (C) is the double layer charge and Q_{ads} (C) is the adsorption charge and other symbols have their usual significances. According to the results shown in Fig. 3F and G, A is calculated to be 0.072 cm^2 and 0.151 cm^2 for bare GCE and AuNPs/WS_2–AB/GCE, respectively. The results indicated that the effective surface area of the electrode increased greatly after modification with AuNPs/WS_2–AB film, which would increase the immobilization amount of the capture DNA and therefore improved the sensitivity of the sensor.

Fig. 3H shows the signal-amplification effect of the as-prepared material. Current signal greatly increases when the WS_2–AB is employed in the sensor construction (curve b). The corresponding signal obtained in the presence of WS_2–AB composites (curve b) is about 214.3% to that in the absence of WS_2–AB composites (curve a), indicating that the WS_2–AB composites are helpful to enhance the detection sensitivity.

3.4. Optimization of experimental conditions

To obtain good analytical performance, several experimental conditions were optimized. The deposition time of AuNPs plays an important role in the size of the AuNPs. The effect of deposition time of AuNPs was tested in the range of 10–120 s (Fig. 4A). The peak current increases in the deposition time range of 10–60 because more and more AuNPs are formed on the electrode. The current response decreases after 60 s due to the formation of the big AuNPs, which reduces the active sites. So 60 s of deposition time was used.

The hybridization reaction temperature on the DPV response was investigated at different temperatures (20, 25, 30, 32, 35, 37, 40, 42, 45, 50 °C) (Fig. 4B). The results show that the DPV response increases

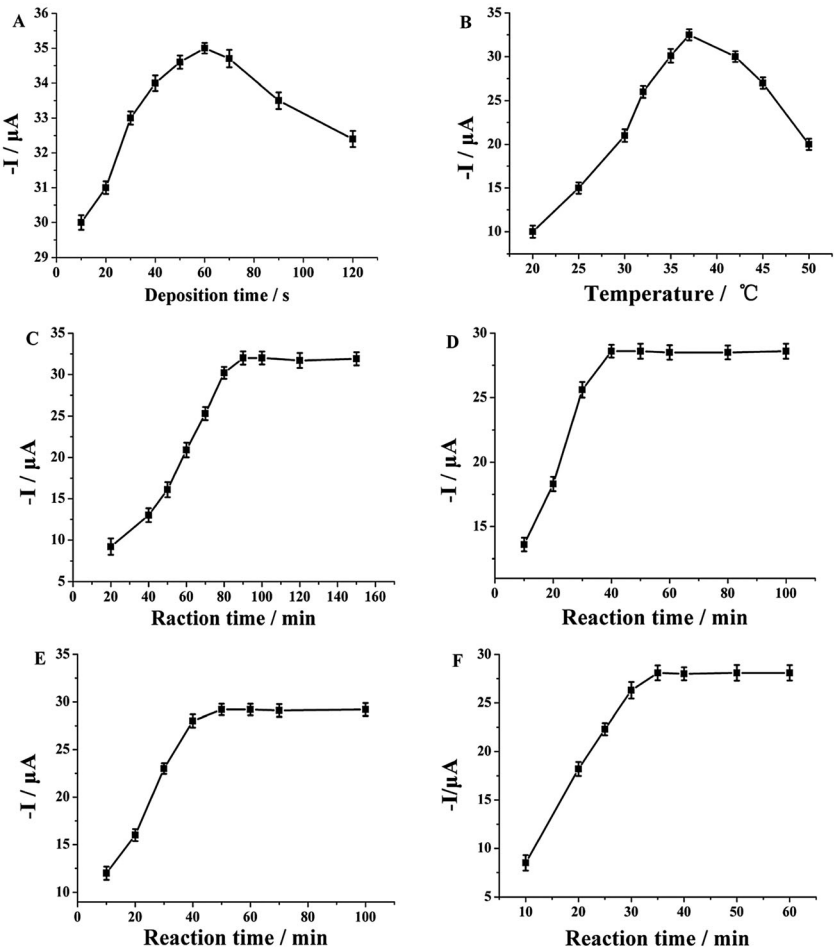

Fig. 4 Effects of deposition time of AuNPs (A), hybridization temperature (B), the hybridization time between the capture probe and target DNA (C), target DNA and auxiliary DNA (D), HCR (E) and self-assembly time of HRP (F) on the peak current.

along with the increase of the reaction temperature in the range of 20–37 °C, indicating the extension of the length of the DNA duplex. The peak current then decreases from 37 to 50 °C because the higher temperature will destroy the DNA duplex construction. So 37 °C was chosen in all subsequent hybridization reactions.

The effect of the hybridization reaction time between the capture probe and target DNA on the DPV response of $[Fe(CN)_6]^{-3/-4}$ was evaluated. As shown in Fig. 4C, the peak current increases rapidly when the reaction time ranges from 20 to 150 min, and almost remains stable after 90 min, suggesting that the hybridization reaction is completed. Thus, 90 min of hybridization reaction time was used. Similarly, the hybridization reaction time between target DNA and auxiliary DNA on the DPV response was also evaluated. As we can see from Fig. 4D, the DPV response intensifies with increasing reaction time and remains constant to a saturation value after 40 min, indicating that a 40 min reaction time is efficient for the hybridization of target DNA and auxiliary DNA.

The HCR time was studied in the range of 10–90 min (Fig. 4E). The result shows that the DPV response increases greatly in the HCR time range of 10–40 min, and then almost remains stable when it exceeds 50 min. This result indicates that the HCR is primitively completed at 50 min. Therefore, 50 min was employed in the subsequent experiments.

Self-assembly time of HRP on the DPV response was also investigated. As shown in Fig. 4F, the DPV response increases gradually with the augment of reaction time and then tends to be constant after 35 min, which indicates that the maximum HRP has been immobilized on the electrode. Thus, 35 min was used.

3.5. Optimization detection system

In this work, the detection system was based on HRP catalysis of the oxidation substrate of H_2O_2 + HQ. Herein, HQ plays as an electroactive mediator of shuttling electrons from the electrode surface to the redox center of HRP. Therefore, the catalytic reduction mechanism of H_2O_2 by the immobilized HRP can be described as follows: firstly, the H_2O_2 substrate is reduced to H_2O by the immobilized HRP in the reduced state (HRP_{Red}), and HRP_{Red} itself will turn into its oxidized state HRP_{Ox}. Then, HQ can reverse HRP_{Ox} back into HRP_{Red} and be oxidized into benzoquinone (BQ). BQ can engage in electron exchange with the electrode and itself turns back into HQ. Therefore, HQ recycles in the system causing the amplification of the reduction current. The reaction mechanism of the catalytic process can be expressed as follows:[32]

$$H_2O_2 + HRP_{Red} \rightarrow HRP_{Ox} + H_2O \quad (2)$$

$$HRP_{Ox} + HQ \rightarrow BQ + HRP_{Red} \quad (3)$$

$$BQ + 2H^+ + 2e \rightarrow HQ \quad (4)$$

The pH of solution and the concentration of the substrate are the important factors influencing the detection sensitivity since pH can affect the biological activity of HRP. The effect of pH was tested in the range of 4–9. The highest DPV response is obtained at pH 7 (Fig. 5A). The effect of H_2O_2 concentration was also studied. As shown in Fig. 5B, the DPV response increases with the increase of H_2O_2 concentration in the range of 0–3.4 mM, and then almost reamins stable when it exceeds 1.8 mM. Similarly, the effect of HQ concentration was evaluated in the range of 0–3.5 mM.

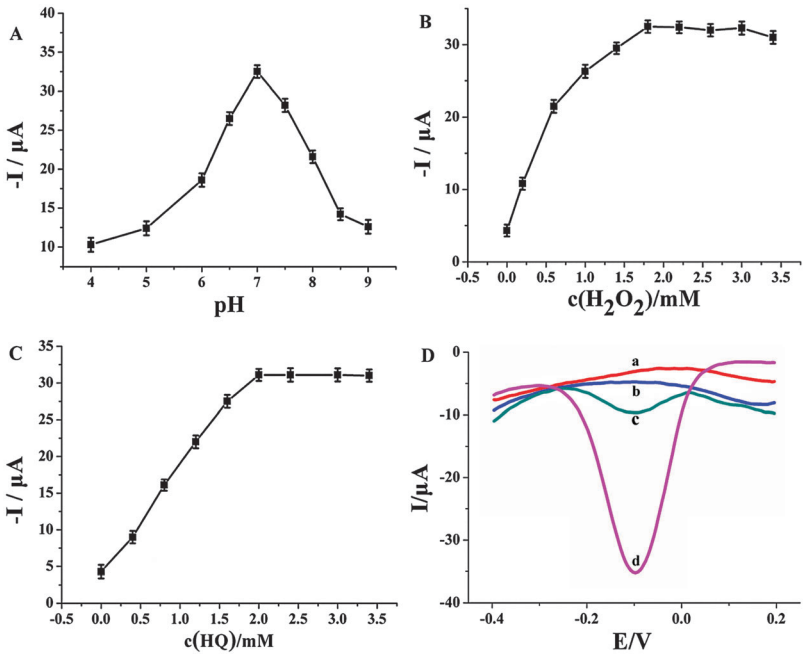

Fig. 5 (A) The current response of the biosensor in PBS containing and 1.8 mM H_2O_2 and 2 mM HQ at different pH values. (B) The current response of the biosensor in PBS (pH 7.0) containing different H_2O_2 concentrations. (C) The current response of the biosensor in PBS (pH 7.0) containing different HQ concentrations. (D) DPVs of HRP/HCR/auxiliary/target/probe/BSA/AuNPs/WS_2–AB/GCE in 0.1 M PBS (7.0) containing 0 (a), 1.8 mM H_2O_2 (b), 2 mM HQ (c) and 1.8 mM H_2O_2 + 2 mM HQ (d). Error bars represent the standard deviation of three repeat measurements.

As shown in Fig. 5C, the current response increases with the increase of HQ concentration in the range of 0–2.0 mM, and then almost reamins stable when it exceeds 2 mM. Thus, 2 mM HQ and 1.8 mM H_2O_2 were selected.

The electrocatalytic activity of the HRP on the electrode toward HQ + H_2O_2 was studied. As seen in Fig. 5D, no redox response is observed in pH 7.0 PBS without H_2O_2 and HQ (curve a) or only with H_2O_2 (curve b). A low reduction peak is obtained when 2.0 mM HQ is added (curve c). Then, when 1.8 mM H_2O_2 + 2.0 mM HQ is added, a significant reduction peak is observed (curve d). On the basis of these results, we might reach a conclusion that the HRP electrode coupled with the HQ + H_2O_2 system could amplify the detection signal.

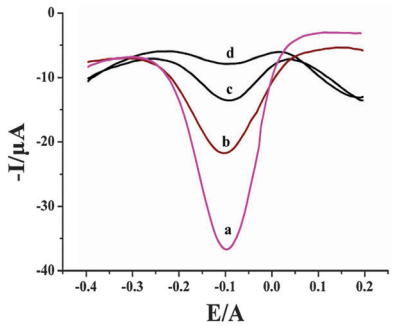

Fig. 6 DPV curves responding to 1 pM target DNA immersed in the mixture of bio-H1 and bio-H2 (a), only immersed in bio-H1 (b), only immersed in bio-H2 (c), and immersed in blank (d).

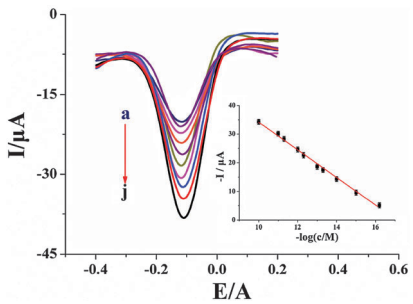

Fig. 7 DPV curves responding to different target DNA concentrations (from a to j): 0, 1.0×10^{-15}, 1.0×10^{-14}, 5.0×10^{-14}, 1.0×10^{-13}, 5.0×10^{-13}, 1.0×10^{-12}, 5.0×10^{-12}, 1.0×10^{-11}, 1.0×10^{-10} M, respectively. Inset: the relationship between the peak current and the negative logarithm of the target DNA concentration.

3.6. The signal amplification effect of the HCR

Herein, a single auxiliary DNA can induce a chain of H1–H2 probes to be hybridized and captured on the electrode surface. H1–H2 probes are labeled by biotin, so they allow further capture of a lot of HRP. HRP can catalyze the inactive HQ to an electrochemically active BQ, which can be detected using DPV. In order to validate the signal amplification effect of HCR, the electrochemical performances of different electrodes were compared. As shown in Fig. 6, the electrode modified with the mixture of bio-H1 and bio-H2 (curve a) shows a much more remarkable signal than the electrode only modified with bio-H1 (curve b), bio-H2 (curve c) and the blank (curve d), which demonstrates that HCR can greatly improve the sensitivity of the sensor.

3.7. Analytical performance of the designed biosensor

Under the optimal conditions, various concentrations of target DNA were detected. Fig. 7 shows that the peak current increases with the increasing concentration of target DNA. There was a good linear relationship between the peak current and the logarithm of the target DNA concentration in the range of 0.001–100 pM. The linear calibration equation was i (μA) = −5.08 log(c/M) − 85.43 (i is the peak current and c is the concentration of target DNA) with a correlation coefficient (R) of 0.997. The detection limit was calculated to be 1.2×10^{-16} M based on three times the standard deviation of the blank sample measurement. The analytical performances of different assays are compared in Table 3. The proposed assay exhibits the lowest detection limit and the widest detection range.

3.8. Specificity, repeatability and stability

In order to validate the selectivity of the developed biosensor, different DNA sequences including the noncomplementary sequence, three-based mismatch sequence, one-based mismatch sequence and the complementary sequence were tested with the developed biosensor. As shown in Fig. 8, the higher peak current is observed when the complementary sequence is used, indicating good specificity of the proposed biosensor.

The reproducibility of the developed biosensor was estimated. The peak currents of ten successive measurements of 1×10^{-14} M target DNA by DPV were determined and a relative standard deviation (RSD) of 2.1% was obtained. Eight parallel-made biosensors were used to detect 1×10^{-14} M target DNA and a

Table 3 Comparison between the proposed assay and other reported methods for DNA detection

Electrodes	Analytical technique	Linear range (nM)	LOD (pM)	Ref.
Phenylenediamine–NH_2/GO/GCE	EIS	0.001–100	0.11	33
Gr–AuNPs/GCE	Amperometric current–time curve	0.00005–100	0.0034	34
Gr/polyaniline/GCE	DPV	0.0001–700	0.032	35
CeO_2–single-walled carbon nanotubes–1-butyl-3-methylimidazolium hexafluorophosphate/GCE	EIS	0.001–100	0.23	36
Chit–CeO_2–ZrO_2/Au	DPV	0.000163–16.3	0.1	37
CeO_2/Chit/GCE	DPV	0.0159–116	10	38
4-Aminothiophenol/AuNPs/Au	DPV	0.014–2	9.5	39
WS_2–Gr/GCE	DPV	0.00001–0.5	0.0023	40
AuNPs/WS_2–AB/GCE	DPV	0.000001–0.1	0.000115	This work

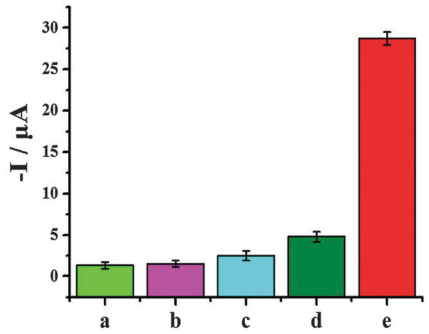

Fig. 8 The specificity of the HCR-based DNA sensor hybridized to different target sequences: blank (PBS 7.0) (a), 1.0×10^{-11} M noncomplementary sequence (b), 1.0×10^{-11} M three-based mismatch sequence (c), 1.0×10^{-11} M one-based mismatch sequence (d) and 1.0×10^{-11} M complementary sequence (e).

RSD of 3.8% was achieved, indicating good reproducibility. The stability of the proposed biosensor was also investigated. When the biosensor was stored at 4 °C for 15 days, it retained 94.6% of its initial current response, indicating good stability.

3.9. Serum samples analysis

In order to verify the general applicability of proposed assay for real-sample analysis, the developed biosensor was used to detect the target DNA in serum samples. The serum sample was diluted to 1 : 10 with PBS (pH 7.0). 0.1 M PBS (pH 7.0) and the serum sample were then spiked with three target DNA concentrations (0.01 pM, 5 pM, 100 pM), respectively. The samples were then detected with the proposed assay. The peak currents of three spiked target DNA concentrations were close in serum (13.6, 20.9, 33.2 μA) and in 0.1 M PBS (14.3, 22.6, and 34.3 μA), which indicated good potential of the developed assay for clinical applications.

4. Conclusions

In summary, an ultrasensitive electrochemical DNA biosensor was developed for the detection of target DNA based on HCR integrating a novel WS_2–AB composite. The WS_2–AB composites possessed large specific surface area and good biocompatibility, which not only increased the immobilization amount of AuNPs and efficiently accelerated the electron transfer, but also retained the active immobilized biomolecules and enhanced the stability of the DNA probe. The proposed DNA sensor showed a low detection limit (0.12 fM), a wide linear range (0.001 M to 100 pM) and satisfactory selectivity. Compared with traditional methods for the synthesis of target DNA, major advantages of the proposed assay are high sensitivity, wide response linearity and rapid readout of target DNA, and it has a great potential for versatile applications in genetic target analysis in bioanalytical and clinical diagnostics and mutation identification.

Acknowledgements

This work was supported by the National Natural Science Foundation of China (U1304214 and 21475115) and Program for University Innovative Research Team of Henan (15IRTSTHN001), Henan Provincial Science and technology innovation team (C20150026), Nanhu Scholars Program of XYNU and Graduate Students Sustentation Fund of Xinyang Normal University (No. 2015KYJJ34).

References

1 X. L. Zhu, L. Y. Sun, Y. Y. Chen, Z. H. Ye, Z. M. Shen and G. X. Li, *Biosens. Bioelectron.*, 2013, **47**, 32.
2 D. F. Luo, X. Liu, L. L. Wang and Z. Z. Ma, *J. Xinyang Norm. Univ., Nat. Sci. Ed.*, 2014, **27**, 538.
3 Z. Y. Peng, B. Young, A. E. Baird and S. A. Soper, *Anal. Chem.*, 2013, **85**, 7851.
4 Z. Y. Peng, S. A. Soper, M. R. Pingle, F. Barany and L. M. Davis, *Anal. Chem.*, 2010, **82**, 9727.
5 J. M. Emory, Z. Y. Peng, B. Young, M. L. Hupert, A. Rousselet, D. Patterson, B. Ellisond and S. A. Soper, *Analyst*, 2012, **137**, 87.
6 Z. Y. Peng, *J. Shihezi Univ., Nat. Sci.*, 2014, **32**, 371.
7 J. M. Emory, Z. Y. Peng, F. Crawford-Drake, P. C. Chen, M. C. Murphy and S. A. Soper, *Twelfth International Conference on Miniaturized Systems for Chemistry and Life Sciences*, San Diego, California, USA, 2008, p. 402.
8 Z. Y. Peng, *Signle-molecule detection of molecular beacons generated from LDR on thermoplastic microfluidic device for bioanalysis*, Doctor thesis, Louisiana State University, Baton Rouge, Louisiana, USA, 2012.
9 Y. Wan, H. Xu, Y. Su, X. H. Zhu, S. P. Song and C. H. Fan, *Biosens. Bioelectron.*, 2013, **41**, 526.
10 W. Ren, Z. F. Gao, N. B. Li and H. Q. Luo, *Biosens. Bioelectron.*, 2015, **63**, 153.
11 K. J. Huang, Y. J. Liu, H. B. Wang, Y. Y. Wang and Y. M. Liu, *Biosens. Bioelectron.*, 2014, **55**, 195.
12 Y. Qian, C. Y. Wang and F. L. Gao, *Biosens. Bioelectron.*, 2015, **63**, 425.
13 S. F. Liu, Y. Wang, J. J. Ming, Y. Lin, C. B. Cheng and F. Li, *Biosens. Bioelectron.*, 2013, **49**, 472.
14 B. P. Ting, J. Zhang, Z. Q. Gao and J. Y. Ying, *Biosens. Bioelectron.*, 2009, **25**, 282.
15 G. Liu, Y. Wan, V. Gau, J. Zhang, L. Wang, S. Song and C. Fan, *J. Am. Chem. Soc.*, 2008, **130**, 6820.
16 H. Li, Z. Sun, W. Zhong, N. Hao, D. Xu and H. Y. Chen, *Anal. Chem.*, 2010, **82**, 5477.
17 Y. Jin, X. Yao, Q. Liu and J. Li, *Biosens. Bioelectron.*, 2007, **22**, 1126.
18 J. Zhao, S. S. Hu, Y. Cao, B. Zhang and G. X. Li, *Biosens. Bioelectron.*, 2015, **66**, 327.
19 Z. L. Ge, M. H. Lin, P. Wang, H. Pei, J. Yan, J. Y. Shi, Q. Huang, D. N. He, C. H. Fan and X. L. Zuo, *Anal. Chem.*, 2014, **86**, 2124.
20 X. Z. Hu, P. Wang, J. Q. Yang, B. Zhang, J. Li, J. Luo and K. B. Wu, *Colloids Surf., B*, 2010, **81**, 27.
21 Y. Y. Zhang, Y. Y. Wang, K. B. Wu, S. C. Zhang, Y. Zhang and C. D. Wan, *Colloids Surf., B*, 2013, **103**, 94.
22 K. J. Huang, Y. J. Liu, J. Z. Zhang, J. T. Cao and Y. M. Liu, *Biosens. Bioelectron.*, 2015, **67**, 184.

23 M. Pumera and A. H. Loo, *Trends Anal. Chem.*, 2014, **61**, 49.
24 K. J. Huang, L. Wang, Y. J. Liu, H. B. Wang, Y. M. Liu and L. L. Wang, *Electrochim. Acta*, 2013, **109**, 587.
25 D. F. Luo and X. Liu, *J. Xinyang Norm. Univ., Nat. Sci. Ed.*, 2015, **28**, 542.
26 J. Li, Z. J. Yang, Y. Tang, Y. C. Zhang and X. Y. Hu, *Biosens. Bioelectron.*, 2013, **41**, 698.
27 H. B. Wang, H. D. Zhang, Z. H. Xing, X. L. Li and Y. Chen, *J. Xinyang Norm. Univ., Nat. Sci. Ed.*, 2015, **28**, 550.
28 H. Liu, D. Su, G. Wang and S. Z. Qiao, *J. Mater. Chem.*, 2012, **22**, 17437.
29 C. B. Zhu, P. Kopold, W. H. Li, P. A. V. Aken, J. Maier and Y. Yu, *J. Mater. Chem. A*, 2015, **3**, 20487.
30 R. Bhandavat, L. David and G. Singh, *J. Phys. Chem. Lett.*, 2012, **3**, 1523.
31 Y. Yong, L. Zhou, Z. Gu, L. Yan, G. Tian, X. Zheng, X. Liu, X. Zhang, J. Shi, W. Cong, W. Yin and Y. Zhao, *Nanoscale*, 2014, **6**, 10394.
32 S. Yang, W. Z. Jia, Q. Y. Qian, Y. G. Zhou and X. H. Xia, *Anal. Chem.*, 2009, **81**, 3478.
33 Y. W. Hu, F. H. Li, D. X. Han, T. S. Wu, Q. X. Zhang, L. Niu and Y. Bao, *Anal. Chim. Acta*, 2012, **753**, 82.
34 K. J. Huang, J. Li, Y. Y. Wu and Y. M. Liu, *Bioelectrochemistry*, 2013, **90**, 18.
35 A. L. Liu, G. X. Zhong, J. Y. Chen, S. H. Weng, H. N. Huang, W. Chen, L. Q. Lin, Y. Lei, F. H. Fu, Z. L. Sun, X. H. Lin, J. H. Lin and S. Y. Yang, *Anal. Chim. Acta*, 2013, **767**, 50.
36 M. Du, T. Yang, X. Li and K. Jiao, *Talanta*, 2012, **88**, 439.
37 W. Zhang, T. Yang, X. Zhuang, Z. Guo and K. Jiao, *Biosens. Bioelectron.*, 2009, **24**, 2417.
38 Q. X. Wang, F. Gao, X. Zhang, B. Zhang, S. X. Li, Z. S. Hu and F. Gao, *Electrochim. Acta*, 2012, **62**, 250.
39 K. J. Feng, Y. H. Yang, Z. J. Wang, J. H. Jiang, G. L. Shen and R. Q. Yu, *Talanta*, 2006, **70**, 561.
40 K. J. Huang, Y. J. Liu, H. B. Wang, T. Gan, Y. M. Liu and L. L. Wang, *Sens. Actuators, B*, 2014, **191**, 828.